Theor Chem Acc (1999) 101:126–130
DOI 10.1007/s00214980m107

Theoretical
Chemistry Accounts

Regular article

Study of flexible joints and permanent bends in DNA fragments by brownian dynamics simulations*

Giuseppe Chirico, Maddalena Collini

Istituto Nazionale di Fisica della Materia, Università degli Studi di Milano, Dipartimento di Fisica, via Celoria 16, I-20133 Milan, Italy

Received: 24 March 1998 / Accepted: 3 September 1998 / Published online: 23 November 1998

Abstract. The use of Brownian dynamics simulations to investigate the presence of structural (kinks) and dynamic (bulges) anomalies in short DNA stretches is analyzed in connection with a string-of-beads model. A scaling method to choose the hydrodynamic translational and rotational parameters of the beads is proposed and tested on straight, kinked and bulged DNA fragments 17 nm long. The model reproduces the rigid-body rotational diffusion for the straight DNA and for the fluorescence polarization anisotropy decay of the kinked and bulged DNAs the model predicts a different behavior which is found experimentally.

Key words: Brownian dynamics – Fluorescence polarization anisotropy – DNA flexibility

1 Introduction

DNA is generally envisioned as a smooth symmetric cylinder and its dynamics is characterized by bending and torsional rigidity. It is known that in the case of base mismatch one expects some dynamic anomalies, such as local enhancement of torsional or bending flexibility. When regular DNA fragments are considered, suitable and robust analytical theories that allow the prediction of several experimental results are available [1–3]. On the other hand, Brownian dynamics (BD) simulations are very useful for analyzing experimental data since no accurate analytical model appears to be available for "anomalous" structures. By modeling DNA as a chain of touching beads, one can simulate the behavior of the correlation functions of several spectroscopic responses. Due to the coarseness of the bead model (each bead encompasses approximately nine base pairs), some effective structural parameters, such as the DNA radius, are needed for the simulation of the uniform motion, i.e. the rigid-body dynamics. The fact that this effective radius does not fit the expected internal dynamics, generally diminishes the power of BD as a tool for quantitatively interpreting the experimental data. The aim of this paper is to show that, by means of a rescaling procedure, it is possible to simulate both the rigid-body motion and the internal dynamics and that it is also possible make a direct comparison with the experimental data.

Fluorescence polarization anisotropy (FPA) has been used as an experimental probe of overall DNA dynamics and as a test for the applicability of BD simulations. The FPA technique has proved to be a sensitive technique for investigating the size and the conformation of short DNA fragments labeled with suitable fluorescent probes [4–6]. We also apply this analysis to experimental data from three different 50-base-pair fragments containing bulged stretches of five base pairs [7]. The effect of loops and bending on short DNA regions has been examined in recent years with a variety of techniques, such as denaturation kinetics [8], gel migration [9], circularization kinetics [7], fluorescence resonance energy transfer [10] and FPA [6]. Bendings and loops are suggested to be correlated to base unpairing and to act by favoring the binding of proteins or the contact between otherwise far apart regions of the DNA helix [11, 12]: it is therefore important to assess the amount and the type of anomaly induced on DNA in solution.

2 Brownian dynamics

The general BD procedure is based on the finite difference method for integrating the Langevin equations for the polymer [13–15] which also takes into account the coupling between the torsional and bending dynamics of DNA [16,17]. The DNA segment is described as a string of touching beads and the bending

* Contribution to the Proceedings of Computational Chemistry and the Living World, April 20–24, 1998, Chambery, France

Correspondence to: G. Chirico
e-mail: chirico@mi.infm.it

and torsional kinematics are described by assigning the positions of the center of each of the M beads and the direction of M-1 reference directions perpendicular to the bonds. These, together with the bond vectors, define a local system of reference centered on each bead: the rotation that brings the $(i-1)$th onto the ith system is given by the Euler rotation $E(\alpha_i,\beta_i,\gamma_i)$. Hydrodynamic interactions are included explicitly in the simulations by computing the Rotne-Praeger tensor [18].

The model structural parameters are the bead's translational diffusion coefficient D_0, the rotational spinning diffusion coefficient of each bond D_R and the bead-bead distance b_0. The choice of the diffusion coefficient is made by keeping the total volume of the string of beads equal to that of the DNA cylinder. This equivalence has been proposed by Hagerman [19] and gives satisfactory agreement between the tumbling diffusion coefficient of the bead chain and of the corresponding cylinder [20]. As an example, a DNA radius $R = 1.3$ nm would correspond to a bead chain with a bead radius $R_{beads} = 1.592$ nm. This scaling imposes some coarseness on the model since only DNA lengths proportional to the bead's radius are possible. In order to choose the spinning diffusion we impose a constraint on the total spinning diffusion of the DNA cylinder. From torsional Langevin dynamics one would predict a total spinning diffusion for the fragment, $D_{spin} = D_R/(M\text{-}1)$, where D_R is the spinning diffusion coefficient of the single bond. This assumes a negligible effect of the bending-torsional coupling on the rigid-body spinning dynamics [16]. On the other hand, one knows accurate expressions for D_{spin} such as those given by Garcia de la Torre [21], where D_{spin} depends on the total DNA length (L) and radius (R):

$$D_{spin} = \frac{K_B T}{\left[3.841\pi\eta L R^2\left(1+\delta_{||}\right)\right]}$$

$$\delta_{||} = (0.677/p) - \left(0.183/p^2\right) \ , \qquad (1)$$

where $p = L/2R$ is the axial ratio, η is the solution viscosity at a temperature T. The D_R value is found by inversion of the equation obtained by comparing the BD (i.e. $D_R/(M\text{-}1)$) and the hydrodynamic (Eq. 1) values of the spinning coefficient. As an example, a 50-base-pair DNA simulated with $M = 5$ beads with $b_0 = 3.184$ nm and $D_R = 50.15$ MHz corresponds to the spinning of a rod 0.34 nm high and with a diameter of approximately 1.3 nm. The same scaling procedure can be repeated when a non-touching-bead model is assumed, such as in simulating long DNA molecules [16]. In this case, beside the choice of the bead's translational diffusion coefficient D_0 and of the spinning diffusion coefficient D_{spin}, one must also scale the dynamic parameters [16]. It is clear, however, that in order to predict details of the DNA structure it is preferable to adopt a touching-bead model.

Harmonic intermolecular potentials take into account the rigidities among the beads through a stretching potential U_s, a bending potential U_b and a torsional potential U_t.

For completeness we give the form of these potentials:

$$U_s = \frac{K_B T}{2\delta^2} \sum_{i}^{M-1} (b_i - b_0)^2 \qquad (2)$$

$$U_b = \frac{K_B T}{2} \sum_{i=1}^{M-2} \frac{1}{\psi_i^2}\beta_i^2 \qquad (3)$$

$$U_t = \frac{K_B T}{2} \sum_{i=1}^{M-2} \frac{1}{\xi_i^2}(\alpha_i + \gamma_i)^2 \qquad (4)$$

where δ is the stretching variance, the bending variances, ψ_i, can be defined in terms of the polymer local persistence lengths P_i through $\psi_i^2 = b_0/P_i$, while the torsional variances, ξ_i, are defined through the local torsional rigidities C_i, $\xi_{i,x}^2 = b_0 k_B T/C_i$. The torsional and bending parameters are position-dependent and they are included in the sum over the number of beads in order to make it possible to employ, when needed, different values of C_i and P_i for each bead.

The computation of the FPA correlation function throughout each simulation is accomplished by performing the following average [6]:

$$r_B(j\delta t) = \frac{1}{(N_m - j - 1)}\frac{1}{(M-1)} \sum_{k=1}^{M-1} \sum_{i=1}^{N_m - j} P_2\left[\cos\left(\Phi_{i,j,k}\right)\right] \ , \qquad (5)$$

where P_2 indicates the second Legendre polynomials, N_m is the number of time steps, M is the number of beads and $\cos(\Phi_{i,j,k}) = \bar{\mu}_k((i+j)\delta t] \cdot \bar{\mu}_k(i\delta t)$, with $\bar{\mu}_k(t)$ indicating the direction of the intercalated ethidium transition dipole at the kth position.

3 Simulation details, data fitting and DNA preparation

BD simulations were performed on a CRAY C92 (CINECA, Istituto Nazionale di Fisica della Materia) with FORTRAN 77 programs developed in our laboratory [16, 17]. BD simulations were obtained by computing trajectories of 750,000 steps, each time step being 6.7 ps, for a total of 5000 ns. The decays of the fluorescence intensities were computed up to approximately 200 ns where, due to the 20 ns lifetime of ethidium, they are negligible. For each simulation the following values of the parameters were kept fixed: solution temperature $T = 297.15$ K, solution viscosity $= 0.9111$ cP and stretching parameter $= 0.01$ which allows the DNA contour length to be kept constant to within about 2% [16]. The number of monomers units, M, the bead diameter size b_0 and the bond spinning diffusion coefficient are determined for each choice of the DNA length and radius as illustrated in sect. 4. In general, different values of the torsional rigidity C (appearing in the BD as the parameter ξ) and of the persistence length P (defined through the parameter ψ) are assigned to each angle.

The anisotropy of the fluorescence of ethidium-DNA complexes, $r(t)$, defined as $r(t) = \left(I_{||}(t) - I_{\perp}(t)\right)/\left(I_{||}(t) + 2I_{\perp}(t)\right)$, is a measure of the different decay rates of the

fluorescence at the two standard polarizations (parallel and perpendicular to the vertical polarization of the exciting beam, $I_{||}(t)$ and $I_{\perp}(t)$, respectively) and contains information about the macromolecular motion.

In the presence of a small free dye contribution, the total anisotropy is given by the intensity-weighted average of the bound and of the free fluorophore [22]. The free dye anisotropy is given by $r_F(t) = r_0 e^{-t/\tau_{rot}}$, where τ_{rot} is taken to be 100 ps [23], $r_0 = 0.4$ and the fractional intensity of the free dye is called I_F.

The FPA decay was measured by detecting the frequency response of the solution to a modulated exciting beam [24]. The fluorescence emission was modulated at the same frequency as the exciting light, phase-shifted with respect to the excitation and reduced in relative amplitude (demodulation). If one defines the phase shift differences and the demodulation ratios between the two polarizations as $\Delta\phi = \phi_{\perp} - \phi_{||}$ and $\Delta M = M_{\perp}/M_{||}$ the relation between the time domain and the frequency domain measurements can be expressed simply by a Laplace transform of the intensity decays at the two polarization conditions, $L(I_{\perp,||})(\omega)$ in the following way [23]:

$$tg[\Delta(\omega)] = \frac{\mathrm{Im}(L(I_{\perp})(\omega))\mathrm{Re}\big(L(I_{||})(\omega)\big) - \mathrm{Re}(L(I_{\perp})(\omega))\mathrm{Im}\big(L(I_{||})(\omega)\big)}{\mathrm{Re}(L(I_{\perp})(\omega))\mathrm{Re}\big(L(I_{||})(\omega)\big) + \mathrm{Im}(L(I_{\perp})(\omega))\mathrm{Im}\big(L(I_{||})(\omega)\big)}$$

$$\Delta M(\omega) = \frac{|L(I_{\perp})(\omega)|}{|L(I_{||})(\omega)|}, \qquad (6)$$

where $\mathrm{Re}[L(I_{\perp,||})(\omega)]$ and $\mathrm{Im}[L(I_{\perp,||})(\omega)]$ represent the real and the imaginary parts of the Laplace transforms and $I_{||}(t) = I_{tot}[1 + 2r(t)]/3$ and $I_{\perp}(t) = I_{tot}[1 - r(t)]/3$. These relations were used in order to make a direct comparison between the experimental data and the BD simulations.

The FPA data were analyzed according to a FORTRAN routine [6]. Ethidium lifetimes were always kept at 22.5 ns and 1.8 ns for the bound and the free species, respectively. Data fitting was accomplished by minimizing the total chi-squared, i.e. the sum of the square of the normalized differences between the experimental and computed phase differences and modulation ratios. The trial phase differences and modulation ratios are the Laplace transform of the fluorescence intensities obtained from the simulated anisotropy [6].

For the FPA measurements, DNA oligonucleotides were synthesized by the phosphotriester method, as previously described [6], and successively purified by gel electrophoresis. The control fragment F0 was obtained by the reaction of two complementary 50-base-pair sequences (seq. 0 and seq. 0c) [6]. The bulged fragment F2 was obtained by annealing two sequences (seq. 5 and seq. 5c) [6] synthesized with five extra adenines in the middle with respect to seq. 0 and seq. 0c. The kinked fragment, which we will refer to as F1, was obtained by the reaction of seq. 5 with seq. 0c [3]. The fragment F1 has a single insertion of five unpaired bases in one strand, while F2 has a double insertion or "bulge" at the center of the double filament [6]. Ethidium bromide (EB, Sigma) was added to DNA samples in a ratio of 1 EB/200 base pairs. Both DNA and EB were dissolved in STE100 Mg buffer (10 mM Tris-HCl at pH = 7.4, 100 mM NaCl, 5 mM $MgCl_2$, 1 mM EDTA).

4 Results

A reference duplex, such as the fragment F0, was simulated by keeping the same values of the rigidities all over the chain (uniform chain). A bent equilibrium structure, expected for the fragment F1, was simulated by means of an additional "kink" potential [6]. A bulged duplex, such as the fragment F2, was simulated by employing lower values for the bending and torsional rigidities at the central bond than those assumed for the rest of the chain. The simulations were first run for a DNA structure with frozen bending motion and then compared to known analytical theories for the torsional dynamics of a DNA chain [3]: very good agreement was obtained.

In Fig. 1 FPA simulated data for bulged chains are shown together with the FPA of a uniform one (continuous lines). The dotted lines show the results for a chain that was modified by a tenfold weaker torsional rigidity of the center of the chain, whereas the dashed lines refer to a chain modified by a tenfold weaker bending flexibility. Both phase and modulation values are higher for the simulated bulged chains than those for the reference uniform chain. Moreover, one notices that the effect of a purely torsional joint is that of shifting the maximum phase difference values to higher modulation

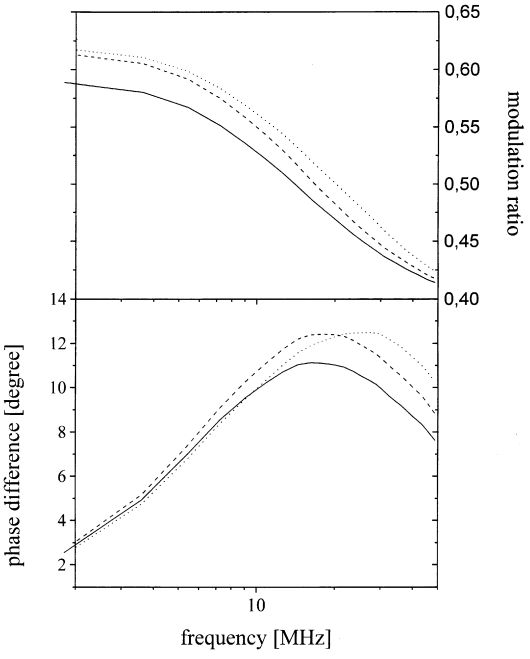

Fig. 1. Fluorescence polarization anisotropy (FPA) data from Brownian dynamics (BD) simulations versus the modulation frequency. *Continuous lines*: uniform chain; $P = 200$ nm, $C = 2.55 \times 10^{-19}$ erg, $M = 5$, $b_0 = 3.184$ nm. *Dotted lines*: chain with torsional joint; same parameters as for the uniform chain and $C_B = C/10$. *Dashed lines*: chain with bending joint; same parameters as for the uniform chain and $P_B = P/10$

frequencies when compared to the uniform chain curve. By computing the spinning and tumbling diffusion coefficients for several configurations that were sampled at random from the BD simulations, it appears that a purely torsional joint does not appreciably modify the rigid-body rotations of the duplex, while a flexible bending joint has considerable effect. In this case the spinning is slower and the tumbling is faster than in the reference "straight" fragment. This effect, however, is much less pronounced than in the case of a bent duplex, where, for instance, the spinning diffusion coefficient was found to be substantially (40%) lower than that of a reference one, depending on the value of the bending angle [6].

It may be of some interest to analyze separately the effect of a torsional and bending joint on either the torsional or the bending internal dynamics. If a fluorescent probe were intercalated with its dipole parallel to the helix axis, the dipole trigonometric factors depending on the intercalation angle ε would cancel the contribution of the twisting correlation functions and, consequently, hinder detection of spinning and torsion. Only bending and tumbling would depolarize the emission in this case. By simulating FPA decay correlation functions with such a probe, ($\varepsilon = 0°$), one could predict the contribution of the bending motions alone to FPA. FPA simulations for a uniform and for a bulged chain where torsional and bending rigidity are reduced fourfold at the bulge site are shown in Fig. 2A.

In order to follow only the torsional dynamics of the fragments, we performed BD simulations for the uniform and the bulged chain with frozen bending motions.

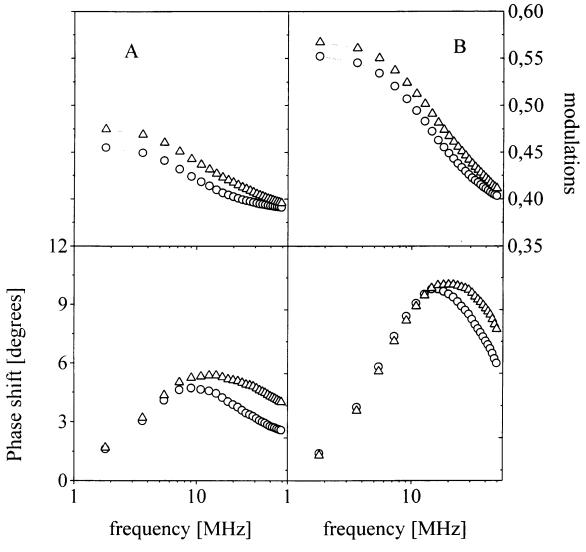

Fig. 2A, B. Effect of a torsional and bending joint on the simulated FPA. The uniform chain (circles) is simulated with $M = 5$, $b_0 = 3.184$ nm, $P = 200$ nm, $C = 2.55 \times 10^{-19}$ erg. The bulged chain is simulated with the parameters of the uniform chain and $C_B = C/4$ $P_B = P/4$ (*triangles*). **A** Effect on the bending dynamics. The two data sets are obtained by setting the transition dipole angle of the fluorescent probe parallel to the helix axis, $\varepsilon = 0$. **B** Effect on the torsional dynamics. The two data sets are obtained by freezing the bending motions as explained in the text

The corresponding FPA simulated curves in the frequency domain are shown in Fig. 2B. The minor differences between the two sets of simulated points show that the effect of the bulge is somewhat smaller on the torsional dynamics than on the bending dynamics. However, it is apparent from Fig. 2 that both types of internal motion provide a significant contribution to FPA.

5 Discussion and conclusions

As a check of the reliability of the BD simulation, we show the direct comparison to the experimental FPA decay of the three fragments F0, F1 and F2. Some simulation parameters were kept fixed: in particular the persistence length is kept at $P = 200$ nm since this value is generally taken to be the most likely [25], and the duplexes studied are short enough not to be influenced by its exact value ($L/P < 0.1$). On the contrary, since torsional rigidity is usually a parameter which is determined from FPA data fitting, in the simulations we have chosen to employ three different values, corresponding to $C = 1.7 \times 10^{-19}$, $C = 2.55 \times 10^{-19}$ and $C = 3.4 \times 10^{-19}$ erg cm (in terms of the torsional constant $\alpha = 5$, 7.5, 10×10^{-12} erg). Least-squares fitting of the simulated FPA data to the experimental FPA correlation functions was done by keeping the limiting dye anisotropy and the free dye fractional contribution as adjustable parameters.

In order to ascertain which value of the spinning radius R better describes the experimental data, in addition to the commonly reported BD value $R = 1.3$ nm, corresponding to $b_0 = 3.184$ nm (i.e. 9.4 base pairs), we also employed $R = 1.1$ nm corresponding to $b_0 = 2.694$ nm; and $R = 1.0$ nm corresponding to $b_0 = 2.45$ nm. The number of bead units employed for the different bead size values was $M = 5$, 6 and 7, respectively. The best chi-squared values for fragment F0 are obtained with a DNA radius of 1.1 nm and uniform rigidity constant values in the range $1.7 \times 10^{-19} \leq C \leq 2.55 \times 10^{-19}$ erg cm corresponding to torsional constants $5 \times 10^{-12} \leq \alpha \leq 7.5 \times 10^{-12}$ erg. The r_0 values fall between 0.360 and 0.375 while I_F ranges from 0.01 to 0.02.

The FPA decay of fragment F1 was fitted to different bent structures as described in detail elsewhere [6], and was found to be compatible with a bending of approximately 45°. Comparison of the experimental to the BD simulation data is shown as triangles in Fig. 3.

For each uniform chain simulation, we have tried a range of likely bulge site rigidities, P_B and C_B, at the central chain angle in order to represent the bulged fragment F2. The values which result in good chi-squared values are those obeying the relations $P_B < P$, $C_B < C$ and $P_B C_B \approx PC/10$, where the values for P and C are those found for the reference fragment F0. The continuous lines in Fig. 3 represent best fits obtained with the BD simulation superimposed on the experimental FPA data. Since in the bead model adopted for the simulation requirements the bulge size comes out larger than the expected size (9.4–8 base pairs out of 47 instead of five base pairs out of 50), the bulge site rigidity

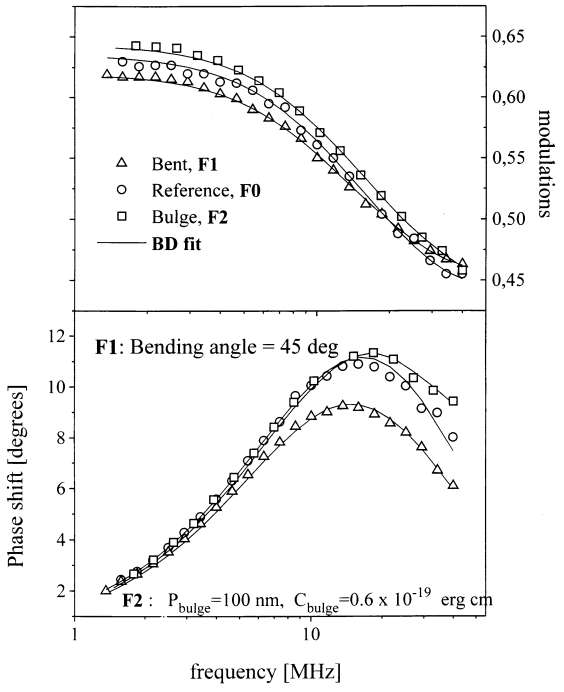

Fig. 3. FPA data for the straight DNA fragment, *F*0 (*circles*), for the DNA fragment with a single insertion, *F*1 (*triangles*), and for the DNA fragment, *F*2 (*squares*), with a double insertion of five base pairs in the middle of the 50-base-pair structure. The *continuous lines* represent BD simulations fitted to the experimental data, according to the following parameters: for *F*0, $R = 1.1$ nm, $P = 200$ nm, $C = 2.55 \times 10^{-19}$ erg, $r_0 = 0.367$, $I_F = 0.02$; for *F*1, $R = 1.1$ nm, $P = 200$ nm, $C = 2.55 \times 10^{-19}$ erg, $r_0 = 0.33$, $I_F = 0.02$, bending angle $\Theta = 45°$; for *F*2, $R = 1.1$ nm, $P = 200$ nm, $C = 2.55 \times 10^{-19}$ erg, $P_B = 1000$ nm, $C_B = 0.64 \times 10^{-19}$ erg, $r_0 = 0.37$, $I_F = 0.017$

values should be rescaled by the ratio of the simulated and the actual bulge sizes. Since the elastic constants (α or P) are inversely proportional to the mean-square angular displacement, which scales with the number of base pairs, one can estimate a scaling factor approximately given by the ratio of base pairs in the two DNA stretches. Our estimate of the bulge torsional and bending rigidities are therefore to be scaled by a factor of 9/5 yielding $P_B C_B \approx PC/(10 \times 1.7^2)$, which is approximately PC/30.

References

1. Barkley MD, Zimm BH (1979) J Chem Phys 70: 2991
2. Allison A, Schurr JM (1979) Chem Phys 41: 35
3. Schurr JM (1984) Chem Phys 84: 71
4. Fujimoto BS, Miller JM, Ribeiro NS, Schurr JM (1993) Rotational dynamics of short DNAs. In: KORPPI-Tommole J EI (ed) Laser Study of Macroscopic Biosystems Proc SPIE 1922: 360
5. Nuutero S, Fujimoto BS, Flynn PF, Reid BR, Ribeiro NS, Schurr JM (1994) Biopolymers 34: 463
6. Collini M, Chirico G, Baldini G, Bianchi ME (1995) Biopolymers 36: 211
7. Kahn JD, Yun E, Crothers DM (1994) Nature 368: 163
8. Crothers DM, Spatz HC (1971) Biopolymers 10: 1949
9. Battacharyya A, Lilley DM (1989) Nucleic Acids Res 17: 6821
10. Lilley DM, Clegg RM (1993) Q Rev Biophys 26: 131
11. Harrington RE (1992) Mol Microbiol 6: 2549
12. Rippe K, Hippel P von, Langowski J (1995) Trends Biochem Sci 20: 500
13. Iniesta A, Garcia de la Torre J (1990) J Chem Phys 92: 2015
14. Ermak DL, McCammon JA (1978) J Chem Phys 69: 1352
15. Fixman M (1978) J Chem Phys 69: 1527
16. Chirico G, Langowski J (1994) Biopolymers 34: 415
17. Chirico G (1996) Biopolymers 38: 201
18. Rotne J, Praeger S (1969) J Chem Phys 50: 4831
19. Hagerman PJ, Zimm BH (1981) Biopolymers 20: 1481
20. Collini M, Chirico G, Baldini G (1996) J Chem Phys 104: 6058
21. Garcia de la Torre J, Bloomfield VA (1981) Q Rev Biophys 14: 81
22. Lakowicz JR (1983) Principles of fluorescence spectroscopy. Plenum, New York
23. Collini M, Chirico G, Baldini G (1992) Biopolymers 32: 1447
24. Lakowicz JR, Maliwal BP (1985) Biophys Chem 21: 61
25. Song L, Schurr JM (1990) Biopolymers, 30: 229